Tuning the dynamics in Fe_3O_4 nanoparticles for hyperthermia optimization

Hao Chen (iD), David Billington, Edward Riordan (iD), Jakob Blomgren (iD), Sean R. Giblin (iD), Christer Johansson (iD), and Sara A. Majetich (iD)

View Online   Export Citation   CrossMark

Tuning the dynamics in Fe_3O_4 nanoparticles for hyperthermia optimization

Hao Chen,[1] David Billington,[2] Edward Riordan,[2] Jakob Blomgren,[3] Sean R. Giblin,[2] Christer Johansson,[3] and Sara A. Majetich[1,a]

AFFILIATIONS

[1]Department of Physics, Carnegie Mellon University, Pittsburgh, Pennsylvania 15213, USA
[2]Department of Physics and Astronomy, Cardiff University, Cardiff CF24 3AA, United Kingdom
[3]Department of Smart Hardware, RISE Research Institutes of Sweden, Göteborg SE-411 33, Sweden

[a]Author to whom correspondence should be addressed: sara@cmu.edu

ABSTRACT

The AC magnetic susceptibility (ACS) of Fe_3O_4 nanoparticles was measured between 10 kHz and 4 MHz at different temperatures and in applied DC fields. In this frequency range, magnetostatic interactions impact magnetization dynamics even for dilute assemblies. The ACS spectrum of relaxation frequencies changes both with temperature and the addition of a small DC field. Because both the relaxation peak frequency and amplitude can be tuned with the DC field, these results could be applied to magnetic hyperthermia applications to optimize heat delivery.

Published under license by AIP Publishing. https://doi.org/10.1063/5.0017903

Iron oxide nanoparticles are under intensive investigation for biomedical applications,[1–4] including magnetic hyperthermia cancer treatment, which use AC magnetic fields for excitation. Despite this, many questions remain about how to optimize the heat delivery.[5–10] Clinical hyperthermia uses a single excitation frequency, most commonly between 100 and 400 kHz, and the efficiency of heating depends on the degree of overlap with the spectrum of relaxation frequencies. The Brownian rotation frequency f_B is on the order of hundreds of kHz or lower, depending on the hydrodynamic diameter, but when particles are taken up by cells, the rotation could be hindered. For an isolated 10 nm particle at 300 K, the Néel relaxation frequency f_N is over 10 MHz.[11] However, when clustered, the resulting magnetostatic interactions can shift f_N and broaden the range of Néel relaxation rates. Here, we describe how magnetostatic interactions impact the real and imaginary parts of the AC magnetic susceptibility, measured over a wide range of excitation frequencies (10 kHz–4 MHz) at different temperatures (100 K–150 K), using a custom-built high frequency AC magnetic susceptibility (ACS) insert for a Quantum Design PPMS,[12] and how the addition of a small DC magnetic field can enhance the response and shift the relaxation peak frequency. While we use a model system of immobilized monodisperse nanoparticles, this approach is general and could be readily adapted for use in clinical applications.

Monodisperse Fe_3O_4 nanoparticles were synthesized by thermal decomposition in a high boiling point organic solvent and coated with a mixture of oleic acid and oleyl amine surfactants. Further synthetic details have been reported previously[13,14] and show a high specific saturation magnetization of $\sim$82 J/Tkg.[15] The particle diameter was found to be (10.7 ± 1.2) nm, based on transmission electron microscopy measurements. The particles were dispersed in melted eicosane (0.15 vol. %) and then cooled to solidify the sample. Electron micrographs, the size distribution analysis, and the zero field cooled (ZFC) and field cooled (FC) magnetization curves are shown in the supplementary material.

In the DC magnetization measurements, the maximum in the ZFC occurs at approximately (105 ± 10) K, and there is a slow drop at higher temperatures. Below the peak, the FC curve is almost constant and the ZFC curve decreases. The gradual decay of the ZFC curve is characteristic of systems with interparticle interactions.[16–18] In a non-interacting model where the peak is at the Blocking temperature, T_B, the anisotropy energy density K estimated from the relation $KV = 25k_BT_B$ would be 5.6×10^4 J/m³, where V is the average particle volume and k_B is the Boltzmann constant. This is higher than that found for ultra-dilute samples of magnetite nanoparticles, $\sim 2 \times 10^4$ J/m³,[9] where the curve drops rapidly above the peak.

The real (χ') and imaginary (χ'') parts of the AC susceptibility reveal the distribution of relaxation frequencies. For these samples in our measurement range, the greatest response was found between 110 and 150 K, at and slightly above the ZFC peak of the DC

measurements. Figure 1 shows the AC magnetic susceptibility components as a function of frequency, for $H_{DC} = 0$, at different temperatures, T. The real part shows a linear decay with frequency, for a logarithmic scale, at 110 K. At higher T, the real part has a more typical roll-off curvature and higher amplitude as fewer spins remain frozen. At lower T, some of the particles are still frozen, while well above it, the particles cannot keep up with the phase of the driving field. At 110 K, the imaginary part shows a very broad peak with a peak frequency at about 100 kHz. At higher temperatures, the dispersive peak sharpens and the peak shifts to higher frequencies. AC hysteresis loops and specific absorption rate (SAR) measurements made with different fixed frequency excitations have also indicated a distribution of relaxation times.[19]

The real and imaginary parts of the magnetic susceptibility can be described by

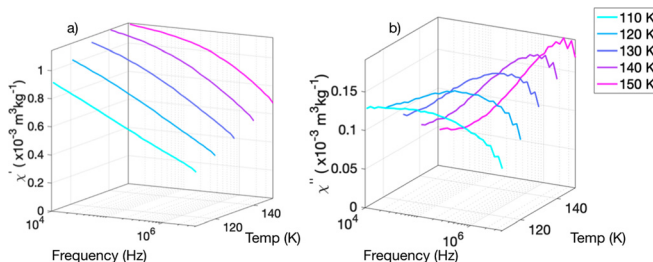$$\chi'(f) = \chi_\infty + \frac{\chi_0 - \chi_\infty}{[1 + (2\pi f\tau)^2]} \quad (1)$$

and

$$\chi''(f) = \frac{(\chi_0 - \chi_\infty)(2\pi f\tau)}{[1 + (2\pi f\tau)^2]}, \quad (2)$$

respectively, where χ_∞ is the infinite frequency susceptibility, χ_0 is the DC susceptibility, and τ is a characteristic relaxation time. $\chi'(f)$ is flat at frequencies where the sample response is in phase with the AC driving field and drops off at higher frequencies as a phase lag develops. $\chi''(f)$ represents the response that is 90° out of phase with the driving field. It rises and peaks at a frequency of $f_c = 1/2\pi\tau$. For *non-interacting* immobilized monodomain particles, τ is often written as

$$\tau = \tau_0 \exp[KV(1 - H/H_K)^2/k_B T], \quad (3)$$

where τ_0 is the Larmor precession time, ~ 1 ns, H is the DC field applied along the particle easy axis, H_K is the anisotropy field, and k_B is the Boltzmann constant. The data of Fig. 1 show qualitatively that f_c increases at higher temperature, as expected. While it is possible to fit χ' and χ'' data at 150 K with the TEM size distribution, there are deviations at lower temperatures. Parameters extracted from fits with a non-interacting model for a single temperature are, therefore, unreliable; further details are provided in the supplementary material.

Interactions of magnetic nanoparticles have been empirically modeled in terms of a Vogel–Fulcher relation[20–22] or a Cole–Cole or Cole–Davidson distribution of relaxation times.[23–25] In the most common form of the Vogel–Fulcher equation, the temperature in Eq. (3) is replaced by the quantity $(T-T_0)$, where T_0 is interpreted as a spin freezing temperature. The origin of this factor was explained in spin glasses
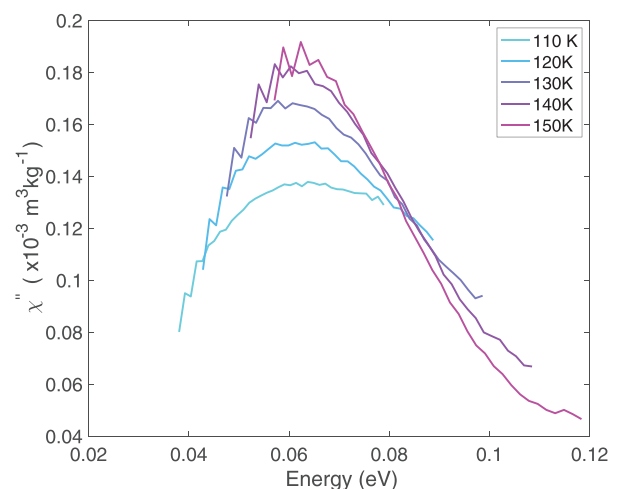
by Shtrikman and Wohlfarth,[26] who assumed a statistical distribution of interaction energies E_{int} and a Langevin function with an average proportional to $\tanh(E_{int}/k_B T) \sim 1/T$. This extra term in the exponential of the Néel–Brown–Arrhenius law leads to the apparent $1/(T- T_0)$ in the Vogel–Fulcher law and $k_B T_0 = E_{int}^2/E$, where E is the Néel–Brown–Arrhenius law energy. Because a Langevin function has an H/T dependence, lowering the temperature or increasing the magnetic field slows down the fluctuation rate. The χ'' data for different temperatures can be scaled with the correct choice of T_0, as shown in Fig. 2, with $T_0 = 30$ K. If $k_B T_0$ is interpreted in terms of the magnetostatic energy of a particle in an average interaction field, $M_s V H_{int}$, where is the saturation magnetization, then $H_{int} \sim 1.5$ mT. This indicates that the energy barrier height KV and the magnetostatic energy $M_s HV$ are of comparable magnitude. At large fields, the latter dominates, and the spins are mainly in the ground state. Ambiguity in the peak frequency of χ'' for 140 and 150 K and the flatness of the 110 K data lead to some uncertainty in estimating T_0. While the peaks of the $\chi''(f)$ data can be scaled with a spin freezing temperature or average interaction energy, real interactions can either increase or decrease the energy barrier. Previous work found $T_0 = 3$ K for 9 nm Fe_3O_4 nanoparticles measured between 0.01 Hz and 1 kHz.[20] Just as the Blocking temperature depends on the measurement time, the use of higher frequencies, probing fluctuations over shorter time scales, leads to a higher spin freezing temperature.

Depending on H, f, and T, different subsets of spins respond to an AC driving field and contribute to the dissipation χ''. The Blocking temperature measured with a slowly varying field depends on the time scale of the measurement. At high temperature, the spins equilibrate within the measurement time, and a superparamagnetic magnetization curve is measured. Below T_B, hysteresis is seen because the response of the spins lags changes in the driving field. $\chi''(f)$ can be viewed as a distribution of Blocking frequencies f_c or the related energy barriers.

The AC susceptibility as a function of a DC magnetic field provides insight into the Blocking frequency distributions. Large DC magnetic fields lock the spins in place, so that they respond minimally to a low amplitude AC driving field, and both χ' and χ'' are very small

FIG. 1. AC susceptibility of the real, χ' (a), and imaginary, χ'' (b), parts vs frequency at different temperatures, with $H_{ac} = 0.045$ mT.

FIG. 2. χ'' data from Fig. 1(b), replotted vs anisotropy energy, taking account of interaction effects assuming a Vogel–Fulcher relation with $T_0 = 30$ K and $\tau_0 = 10^{-9}$ s.

across the entire frequency range. However, for smaller DC fields, surprising non-monotonic behavior is observed, as shown in Fig. 3. At 140 K, both the amplitude of the real part and the relaxation peak frequency changed non-monotonically with H_{dc}. Below 1.25 mT, the peak frequency decreases and the χ'' amplitude increases with increasing DC fields. At and above 1.25 mT, these trends reverse. The dissipation at 100 kHz increases by a factor of 3.8 between 0 and 1.25 mT. We note that 1.25 mT is very close to H_{int} estimated for with Vogel–Fulcher scaling (about 1.5 mT).
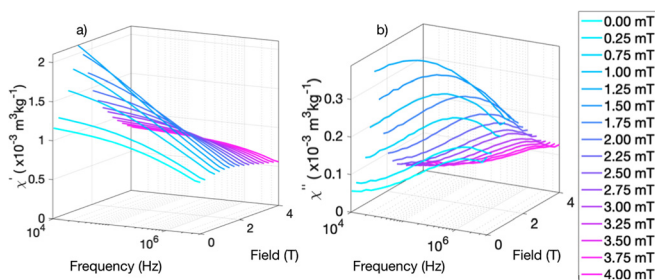
Cole–Cole analysis of χ'' vs χ' data from Fig. 3 was used to get a more accurate estimate of the average relaxation time τ and the relaxation time distribution. For non-interacting particles, a Debye model such as that described in Eqs. (1) and (2) applies, and the Cole–Cole plot will be a semicircle with a peak at τ. In cases where the center of the circle is depressed below $\chi'' = 0$, the data can be fit with an empirical parameter α associated with a distribution of relaxation times,

$$\chi(f) = \chi_{\infty} + \frac{\chi_0 - \chi_{\infty}}{1 + (2\pi i f \tau)^{(1-\alpha)}}. \tag{4}$$
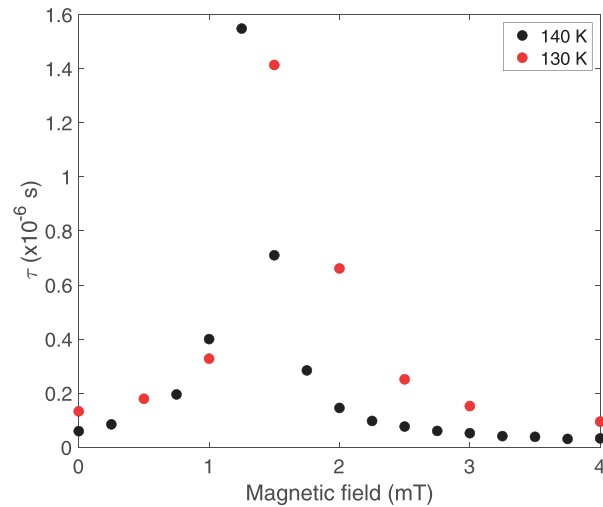
Representative fits of the Cole–Cole plots are shown in the supplementary material, and Fig. 4 summarizes the results as a function of H_{dc}. The average τ is sharply peaked and is nearly 20 times larger at 1.25 mT than at $H = 0$. α was found to vary between 0.46 and 0.67. While care should be taken in the quantitative interpretation of α, its non-zero value shows that magnetostatic interactions impact the relaxation time. τ tracks the peak frequency χ'', and the relative width of the distribution associated with α is the greatest at 1.25 mT, consistent with the data of Fig. 3(b).

In the uniaxial case with the DC field applied along the easy axis, the application of a small field would increase some energy barriers and decrease others, broadening the distribution of relaxation rates. However, the particles are randomly oriented relative to each other and to the applied field. Even if a small amount of shape anisotropy made them effectively uniaxial when isolated,[27] with magnetostatic interactions, the energy landscape is complex, with many local minima. Dipolar interactions among nanoparticles can lead to DC hysteresis characteristic of a soft ferromagnet, with a steeper rise in M(H) and the development of a small coercivity.[28] In the assembly of iron oxide nanoparticles studied here, the effect of a small H_{dc} is to orient more of the moments preferentially, and so they respond to the AC field and dissipate energy.

We have shown that magnetostatic interactions of nanoparticles affect the AC susceptibility even for low concentrations and the

FIG. 4. Extracted value of τ as a function of the DC field, at 130 K (red) and 140 K (black).

limitations of fitting temperature-dependent data with a consistent set of parameters when interactions are ignored (see the supplementary material). While interactions broaden the range of frequencies, the magnitude and peak frequency of χ'' can be tuned using a small DC field comparable to the average interaction field. While we demonstrated this effect for a relatively dilute sample of 10 nm particles at low temperature, it should also be present for more concentrated samples at clinical hyperthermia temperatures, using size and/or shape anisotropy to tune the zero field thermal stability parameter, $\Delta = KV/k_B T$. Our approach combines AC susceptibility measurements with a variable H_{dc} to quantify the effect of magnetostatic interactions, enabling the peak frequency and amplitude to be tuned. In the future, this concept could be used to maximize the SAR for a single excitation frequency. Magnetic particle imaging (MPI), which uses low frequency AC excitation together with spatial gradients of DC magnetic fields,[29] shows that incorporating H_{dc} in a clinical environment is feasible, and it could similarly be combined with existing hyperthermia equipment.[30,31]

See the supplementary material for further information about the particle size distribution, zero field-cooled and field-cooled magnetization, fitting to a non-interacting particle model, field-dependent AC susceptibility, and Cole–Cole model fitting.

DATA AVAILABILITY

The data that support the findings of this study are available from the corresponding author upon reasonable request.

FIG. 3. Real, χ' (a), and imaginary, χ'' (b) susceptibility vs frequency at 140 K at different DC fields, parallel to the AC fields. [In the supplementary material, Fig. S4 shows a 2D projection of data for (b)].

REFERENCES

[1]Q. A. Pankhurst, J. Connolly, S. K. Jones, and J. Dobson, J. Phys. D: Appl. Phys. **36**, R167 (2003).
[2]K. M. Krishnan, IEEE Trans. Mag. **46**, 2523 (2010).

[3]I. Torres-Diaz and C. Rinaldi, Soft Matter **10**, 8584 (2014).

[4]Q. A. Pankhurst, N. T. K. Thanh, S. K. Jones, and J. Dobson, J. Phys. D: Appl. Phys. **42**, 224001 (2009).

[5]M. Kallumadil, M. Tada, T. Nakagawa, M. Abe, P. Southern, and Q. A. Pankhurst, J. Magn. Magn. Mater. **321**, 1509 (2009).

[6]S. Ruta, O. Hovorka, and R. Chantrell, Sci. Rep. **5**, 9090 (2015).

[7]G. Vallejo-Fernandez and K. O'Grady, Appl. Phys. Lett. **103**, 142417 (2013).

[8]H. Sohn and R. H. Victora, J. Appl. Phys. **107**, 09B312 (2010).

[9]E. A. Périgo, G. Hemery, O. Sandre, D. Ortega, E. Garaio, F. Plazaola, and F. J. Teran, Appl. Phys. Rev. **2**, 041302 (2015).

[10]I. M. Obaidat, V. Narayanaswamy, S. Alaabed, S. Sambasivam, and C. V. V. Muralee Gopi, Magnetochemistry **5**, 67 (2019).

[11]S. Bogren, A. Fornara, F. Ludwig, M. Del Puerto Morales, U. Steinhoff, M. F. Hansen, O. Kazakova, and C. Johansson, Int. J. Mol. Sci. **16**, 20308 (2015).

[12]E. Riordan, J. Blomgren, C. Jonasson, F. Ahrentorp, C. Johansson, D. Margineda, A. Elfassi, S. Michel, F. Dell'ova, G. M. Klemencic, and S. R. Giblin, Rev. Sci. Instrum. **90**, 073908 (2019).

[13]S. Sun, H. Zeng, D. B. Robinson, S. Raoux, P. M. Rice, S. X. Wang, and G. Li, J. Am. Chem. Soc. **126**, 273 (2004).

[14]Z. Nedelkoski, D. Kepaptsoglou, L. Lari, T. Wen, R. A. Booth, S. D. Oberdick, D. Gilks, Q. M. Ramasse, R. F. L. Evans, S. A. Majetich, and V. K. Lazarov, Sci. Rep. **7**, 45997 (2017).

[15]F. Ludwig, C. Balceris, T. Viereck, O. Posth, U. Steinhoff, H. Gavilan, R. Costo, L. Zeng, E. Olsson, C. Jonasson, and C. Johansson, J. Magn. Magn. Mater. **427**, 19 (2017).

[16]S. A. Majetich and M. Sachan, J. Phys. D **39**, R407–R422 (2006).

[17]J. M. Vargas, W. C. Nunes, L. M. Socolovsky, M. Knobel, and D. Zanchet, Phys. Rev. B **72**, 184428 (2005).

[18]F. Fabris, K.-H. Tu, C. A. Ross, and W. C. Nunes, J. Appl. Phys. **126**, 173905 (2019).

[19]E. Garaio, J. M. Collantes, F. Plazaola, J. A. Garcia, and I. Castellanos-Rubio, Meas. Sci. Technol. **25**, 115702 (2014).

[20]J. Zhang, C. Boyd, and W. Luo, Phys. Rev. Lett. **77**, 390 (1996).

[21]M. Garcia del Muro, X. Batlle, and A. Labarta, J. Magn. Magn. Mater. **221**, 26 (2000).

[22]X. X. Zhang, G. H. Wen, G. Xiao, and S. Sun, J. Magn. Magn. Mater. **261**, 21 (2003).

[23]P. C. Fannin, S. W. Charles, C. M. Oireachtaigh, and S. Odenbach, J. Magn. Magn. Mater. **302**, 1 (2006).

[24]G. Bellizzi, O. M. Bucci, and A. Capozzoli, J. Magn. Magn. Mater. **322**, 3004 (2010).

[25]K. M. Chowdary and S. A. Majetich, J. Phys. D: Appl. Phys. **47**, 175001 (2014).

[26]S. Shtrikman and E. P. Wohlfarth, Phys. Lett **85**, 467 (1981).

[27]A. A. McGhie, C. Marquina, and K. O'Grady, J. Phys. D: Appl. Phys. **50**, 455003 (2017).

[28]K. Yamamoto, S. A. Majetich, M. R. McCartney, M. Sachan, S. Yamamuro, and T. Hirayama, Appl. Phys. Lett. **93**, 082502 (2008).

[29]B. Gleich and J. Weizenecker, Nature **435**, 1214 (2005).

[30]D. Hensley, Z. W. Tay, R. Dhavalikar, B. Zheng, P. Goodwill, C. Rinaldi, and S. Conolly, Phys. Med. Biol. **62**, 3483 (2017).

[31]E. Myrovali, N. Maniotis, T. Samaras, and M. Angelakeris, Nanoscale Adv. **2**, 408 (2020).